B-Side Electron Transfer in the HE(M182) Reaction Center Mutant from *Rhodobacter sphaeroides*

Evaldas Katilius,* Zivile Katiliene, Su Lin, Aileen K. W. Taguchi, and Neal W. Woodbury

Department of Chemistry and Biochemistry and the Center for the Study of Early Events in Photosynthesis, Arizona State University, Tempe, Arizona 85287-1604

Received: June 26, 2002; In Final Form: September 18, 2002

The histidine (H) ligand of the bacteriochlorophyll monomer molecule on the B-side of the photosynthetic reaction center (RC) from *Rhodobacter (Rb.) sphaeroides* was replaced with a glutamic acid residue (E) (mutant HE(M182)). The photochemical properties of this mutant are markedly different from those of wild-type RCs. The excited state of the initial electron donor (P*) decays with a lifetime of 2.8 ± 0.1 ps, which is about 10% faster than in wild-type RCs. The faster decay of the excited state is due to an additional electron-transfer pathway in the mutant from P to the monomer bacteriochlorophyll on the B-side (B_B) of the RC, forming the state $P^+B_B^-$. The initial yield of the B-side electron transfer is estimated at about 35%, whereas the remaining 65% of P* leads to electron transfer along the A-side pigments forming the charge-separated state $P^+H_A^-$. The $P^+B_B^-$ state formed during initial charge separation decays with a lifetime of 45 ps. Of the 35% $P^+B_B^-$ initially formed, 10% decays to form $P^+H_A^-$ via back electron transfer to P* and subsequent A-side charge separation. The other 25% of the state $P^+B_B^-$ recombines to the ground state. There is no observable further electron transfer from $P^+B_B^-$ to the B-side bacteriopheophytin molecule, H_B. Apparently, $P^+H_B^-$ is at least as high in free energy as is $P^+B_B^-$ in this mutant, preventing further B-side electron transfer. From analysis of the long-lived fluorescence kinetics and transient absorbance data, the standard free energy of the state $P^+B_B^-$ in the HE(M182) mutant is estimated to be 70 meV below P*. Thus, the standard free energy of the state $P^+H_B^-$, which should be similar in the mutant and the wild-type RCs, is apparently less than or equal to 70 meV below P*.

Introduction

The photosynthetic reaction center (RC) is the pigment−protein complex responsible for the primary solar energy conversion reactions of photosynthesis. It accomplishes this via a series of light-driven electron transfer reactions, resulting in transmembrane charge separation. The most extensively studied photosynthetic reaction centers are those from the purple nonsulfur photosynthetic bacteria such as *Rhodobacter* (*Rb.*) *sphaeroides.*[1−3] The RCs from this species of bacteria consist of three protein subunits L, M, and H, which bind 10 cofactors: 4 bacteriochlorophylls (BChl), 2 bacteriopheophytins (BPheo), 2 quinone molecules, a carotenoid molecule, and a nonheme iron. Upon excitation of the initial electron donor, a pair of bacteriochlorophylls (P), to the first excited singlet state (P*), an electron is transferred from P to the initial electron acceptor H_A in about 3 ps, presumably via B_A. Subsequently, the electron is transferred to the primary quinone acceptor, Q_A, in about 200 ps and then to the secondary quinone acceptor Q_B in about 200 μs with an overall quantum yield of nearly unity.[4]

The initial electron transfer in the bacterial photosynthetic reaction center occurs almost exclusively along the cofactors on the A side,[5,6] even though the BChl, BPheo, and quinone cofactors are arranged in two nearly symmetric branches (usually labeled A and B). The quasisymmetric arrangement of the 4 BChl cofactors is facilitated in part by the symmetric histidine ligands on the L and M protein subunits. Extensive studies have been performed to investigate the role of the ligands of all four BChl molecules in the RC.[7−14] The nature of these ligands can be considerably varied, while still maintaining stable association of bacteriochlorophyll with the RC. However, certain amino acid changes do cause alterations in the RC cofactor composition. Mutating the histidine (H) ligand to a leucine (L) or phenylalanine (F) at most positions results in replacement of bacteriochlorophyll with bacteriopheophytin.[7,9,15,16] For example, mutation of histidine M182, a ligand to the monomer bacteriochlorophyll molecule on the B-side (B_B), to leucine (mutation HL(M182)) causes B_B to be replaced with a bacteriopheophytin (called ϕ_B). In this mutant, a 35% yield of B-side electron transfer is observed forming $P^+\phi_B^-$, presumably because the new bacteriopheophytin is considerably easier to reduce than the original bacteriochlorphyll.[16] However, electron transfer does not continue farther along the B-side cofactor chain from the exchanged pigment ϕ_B to H_B because the standard free energy of the state $P^+\phi_B^-$ is apparently lower than that of the state $P^+H_B^-$.[16,17]

To further investigate the energetics of the charge-separated states involving B-side RC cofactors, a histidine to glutamic acid mutation at position M182 has been constructed (mutant HE(M182)). It was anticipated that this mutation might result in the replacement of B_B with BPheo, as seen in HL(M182), and/or perturb the energetics of the states $P^+B_B^-$ or $P^+\phi_B^-$. Analysis of this mutant should allow further characterization of the thermodynamic parameters that control B-side electron transfer in the bacterial reaction centers.

Materials and Methods

The HE(M182) mutation was constructed using a QuikChange site-directed mutagenesis kit (Stratagene). The mutagenesis reaction was performed on the plasmid pUCHBH7, which

* To whom correspondence should be addressed. Fax: (480) 965-2747. E-mail: Evaldas@asu.edu.

10.1021/jp026388x CCC: $22.00
Published on Web 11/02/2002

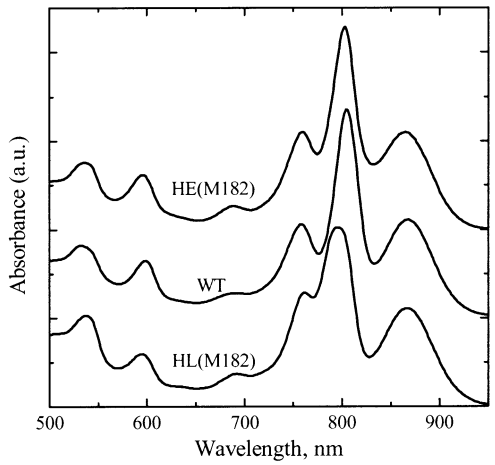

Figure 1. Absorption spectra of reaction centers from the HE(M182) mutant, wild type (WT), and the HL(M182) mutant at room temperature. The spectra were normalized at the maximum of the P band (around 865 nm) and then offset for ease of comparison.

consists of the plasmid pUC19 with the *Hin*dIII-*Bam*HI fragment of the M protein subunit gene inserted into the multiple cloning site.[18] Also, at the end of the M subunit gene, a His-tag sequence (repeat of 7 CAC codons encoding a poly-histidine tag) was added. The mutagenesis reaction was performed according to the kit manual, and the mutation was verified by DNA sequencing of the whole *Hin*dIII-*Bam*HI fragment of the M subunit gene. This fragment was then subcloned into the plasmid pRKSCH, which was transferred by conjugation into the *Rb. sphaeroides* pufLM deletion strain ΔLM1.1, which lacks the reaction center gene.[18,19] Cells were grown and reaction centers were isolated according to previously described procedures.[17] The sample preparation for transient absorbance and time-correlated single photon counting measurements as well as the instruments used have been described previously.[16,17]

Results

Ground-State Spectral Changes. Replacement of B_B with a BPheo molecule (ϕ_B) in HL(M182) mutant RCs results in the disappearance of the B_B absorption bands near 807 and 600 nm and the appearance of a new transition associated with ϕ_B near 785 and 540 nm.[16] However, in the HE(M182) mutant, the spectral changes expected for replacement of B_B with BPheo are not observed (see Figure 1). Instead, the absorption spectrum of HE(M182) RCs at room temperature looks more similar to the WT RC spectrum, though there are several small changes. The maximum of the P band at around 865 nm is shifted by about 3 nm to shorter wavelength. The maximum of the monomer BChl band at around 800 nm is also blue-shifted by about 1 nm, whereas the BChl Q_X band near 600 nm is blue-shifted by roughly 5 nm.

Pigment Composition. The presence of BChl in the B_B binding site is confirmed by pigment analysis. The BChl:BPheo pigment ratio in this mutant is 1.9 ± 0.1, which is the same as in WT RCs. Thus, the mutation of histidine to a glutamic acid does not cause the replacement of BChl with BPheo at the B_B position.

Transient Absorbance Kinetics. Despite the fact that the pigment composition of the HE(M182) mutant is the same as WT RCs, the photochemical properties of the mutant are quite distinct. Transient absorption measurements of the HE(M182) mutant RCs at room temperature show that the P* stimulated emission decay is faster than in WT RCs: 2.8 ± 0.1 ps compared to 3.1 ± 0.2 ps in WT RCs. This indicates that either the primary electron-transfer rate in this mutant is faster or that there is an additional pathway for the decay of the excited state of P.

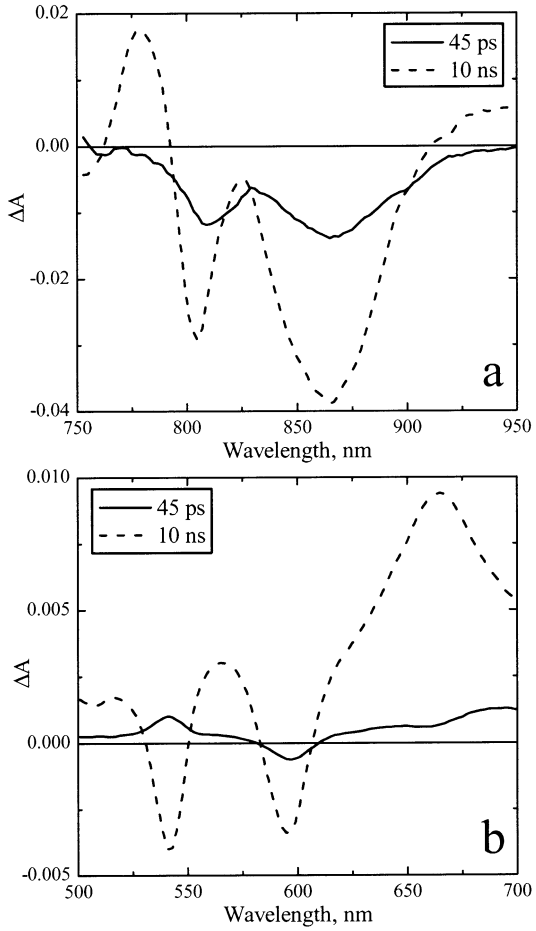

Figure 2. Decay-associated spectra (DAS) that result from global analysis of the time-resolved spectra of quinone-reduced HE(M182) RCs upon 860 nm excitation at room temperature. The transient absorbance spectra were measured over 800 ps delay interval and fitted with a three exponential decay function. The spectra of only the 45 ps and long-lived components are shown; the spectrum of the first decay component with the lifetime of 2.8 ps is essentially identical to that seen in WT RC and is not shown. The lifetime of the long-lived component was fixed at 10 ns during fitting; this component represents the charge-separated state $P^+H_A^-$. Panel a shows DAS in the Q_Y transition region and panel b shows DAS in the Q_X transition region.

In addition to having a faster rate of P* decay, the HE(M182) mutant also shows a significant ground-state recovery of P with a 45 ± 3 ps lifetime. This process is both kinetically and spectrally distinct from the secondary electron transfer from H_A to Q_A, which in this mutant occurs with the same rate constant $(\sim 200 \text{ ps})^{-1}$ as in WT RCs (data not shown). It should be noted that in WT RCs there is no loss of P^+ (no P ground-state recovery) observed on the 200 ps time scale during electron transfer from H_A to Q_A as indicated by constant bleaching at around 865 nm. This behavior, an increase in the decay rate constant of P* and the recovery of the P ground-state absorbance on a longer time scale, is similar to what has been observed in the HL(M182) mutant and attributed to appearance of a new B-side charge separation pathway from P* followed by the charge recombination of the B-side charge-separated state.[16]

Spectral Properties of the Charge-Separated States. To better characterize the properties of the 45 ps transient state in the HE(M182) mutant, transient absorbance spectra were measured in a sample in which Q_A was prereduced (Figure 2).

In WT RCs with prereduced Q_A, the $P^+H_A^-$ state is formed within a few picoseconds after excitation and later decays with a roughly 10 ns lifetime at room temperature.[20] However, in the HE(M182) mutant, the same partial decay of the bleaching of the P band is observed as was described above for unreduced samples. Apparently, about 25% of the P ground-state bleaching at 865 nm decays with the 45 ps lifetime independent of the state of Q_A. The remaining 75% of P bleaching is stable for longer than one nanosecond, and the decay-associated spectrum of this long-lived component corresponds to the transient spectrum of the $P^+H_A^-$ state (see Figure 2a). In addition to the bleaching of the P band, the decay-associated spectrum of the 45 ps component also includes bleaching of the band at 807 nm. This suggests that the transient state decaying on this time scale involves P and B_B, because the BChl molecule in the B_B binding site is shown to absorb near 807 nm.[20] In fact, the spectrum of this 45 ps component is very similar to that previously observed for the charge-separated state $P^+B_A^-$,[21] with the exception that the bleaching near 800 nm associated with B_A^- is replaced by a bleaching near 807 nm.

Transient absorbance spectra measured in the 500−700 nm region support the assignment of the 45 ps component to the decay of the state $P^+B_B^-$ (Figure 2b). The bleaching near 595 nm in the 45 ps decay-associated spectrum again shows that there is recovery of BChl ground-state bleaching on this time scale, consistent with recovery of the P band near 865 nm and the B_B band near 807 nm described above. In addition, a positive band near 690 nm indicates the involvement of the BChl anion.[22]

There is no evidence for a negative feature near 530−540 nm (Q_X transitions of BPheo) in the decay-associated spectrum of the 45 ps component (Figure 2b). There is also no distinct positive feature in the 630 or 660 nm region of the 45 ps decay-associated spectrum, as would be expected for the anions of H_B or H_A, respectively.[23,24] This is consistent with the notion that the state decaying on this time scale does not involve the disappearance of a BPheo anion. Instead, a distinct *increase* in the amount of BPheo ground-state bleaching is observed on this time scale. This increase is evident in the 45 ps decay-associated spectrum as a positive feature centered at 540 nm, the position of the Q_X absorption band of H_A.[20,23−25] This suggests that additional H_A^- is formed on this time scale.

Measurements of Long-Lived Fluorescence from P*. The observations presented above suggest that there is a substantial amount of B-side charge separation occurring in HE(M182) reaction centers upon excitation of P, apparently forming $P^+B_B^-$. Once formed, this charge-separated state appears to decay on the 45 ps time scale. The energetics of the $P^+B_B^-$ state is of considerable interest, as the transient absorbance measurements indicate that there is no further electron transfer to H_B, whereas there is a significant increase of H_A bleaching occurring during the decay of $P^+B_B^-$. Past measurements have shown that it is possible to estimate the energy of charge-separated states formed in the reaction center by monitoring the long-lived fluorescence due to charge recombination reforming P*.[17,26−30] The fluorescence kinetics from quinone-reduced HE(M182) RCs at room temperature were measured using time-correlated single photon counting. The kinetics were fitted with the sum of four exponential decay components to achieve the best fit based on the analysis of the residuals as well as the reduced χ^2 value. The same measurements and analysis were also performed on WT RCs, so that a direct comparison of the kinetics could be performed.

The fitting results for the fluorescence data from HE(M182) and WT are shown in Table 1. For both WT and HE(M182) RCs, the prompt fluorescence decay time is limited by the instrument response function; therefore, the lifetimes of the first components were fixed at the values acquired from the transient absorption results: 2.8 ps for the HE(M182) mutant and 3.1 ps for WT. The lifetimes and amplitudes of other components show that there are two significant differences between the samples. First, although the lifetimes of the third and fourth components are about the same within the error of the measurement, the amplitudes of these two decay components are only about 60% as large in the mutant as in WT RCs. This is consistent with a decrease in the amount of long-lived $P^+H_A^-$ formed in the mutant. Second, the lifetime of the second fluorescence decay component is substantially shorter in HE(M182) RCs than in WT RCs (110 and 150 ps, respectively) and smaller but significant changes are observed in the amplitudes. The interpretation of this involves multiple states and processes that are at play during the early part of the fluorescence decay, and this will be considered in more detail below.

TABLE 1: Fluorescence Kinetics of HE(M182) and WT RCs at Room Temperature[a]

sample	τ_1, ps	A_1, %	τ_2, ps	A_2, %	τ_3, ns	A_3, %	τ_4, ns	A_4, %	χ^2
HE(M182)	2.8	99.3493	110	0.5387	1.0	0.0824	6.0	0.0296	1.08
WT	3.1	99.1991	150	0.6031	0.9	0.1472	5.7	0.0506	1.1

[a] The lifetimes and amplitudes are the results of fitting the fluorescence kinetics measured at 900 nm. The amplitudes were normalized to 100%. The lifetimes of the first components for both samples were fixed using values measured by transient absorption, as the time resolution of the time correlated single photon counting instrument does not allow their accurate determination. The errors of the other fitted lifetimes were estimated to be less than 10%.

Discussion

HE(M182) Reaction Centers Undergo B-side Charge Separation Forming $P^+B_B^-$. Though the pigment composition of HE(M182) RCs is the same as the WT, the spectral and kinetic properties are significantly different. Excitation of the initial electron donor P in the HE(M182) mutant RCs at room temperature gives rise to an additional electron-transfer pathway. Apparently, the charge-separated state $P^+B_B^-$ is formed during initial electron transfer; the evidence for this includes ground-state bleaching of both P (595 and 865 nm) and B_B (595 and 807 nm) and formation of the bacteriochlorophyll anion band at 690 nm, as expected for B_B^- (see Figure 2).[24] This state is formed during the 2.8 ps decay of P* and later decays with a 45 ps time constant at room temperature. However, electron transfer does not appear to continue farther along the B-side cofactor chain from $P^+B_B^-$ to form $P^+H_B^-$ in the HE(M182) mutant. Instead, the development of additional bleaching at 540 nm during the decay of $P^+B_B^-$ is observed (see Figure 2b). These changes are characteristic of additional H_A^- formation on this time scale, as H_B^- formation should be accompanied by bleaching of the 530 nm transition. No bleaching of the H_B band at 530 nm is observed within the accuracy of the measurement.

B-side electron transfer in certain other mutants has resulted in transfer at least as far as H_B or even to Q_B.[24,25,31−35] Multiphoton excitation of R-26 reaction centers induced roughly 30% electron transfer along the B-side and excitation of WT RCs with 390 nm light also showed the formation of a charge-separated state involving H_B, though the mechanism of electron transfer along the B-side in this case must be quite different.[36,37] The absence of electron transfer past $P^+B_B^-$ in the HE(M182) mutant is presumably due to the slow secondary electron transfer

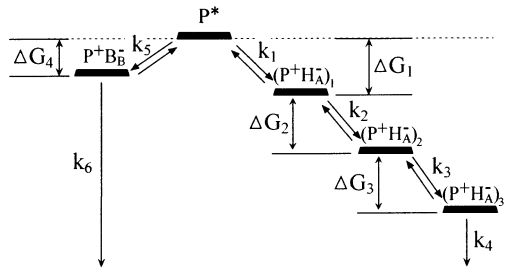

Figure 3. State diagram defining the kinetic and thermodynamic parameters used in the target analysis. P*: excited state of RC initial electron donor. $P^+H_A^-$: charge-separated state of the RC (three different forms are shown denoted with subscripts representing energetically distinct conformations). $P^+B_B^-$: the B-side charge-separated state observed in the HE(M182) mutant. The k_i represent the rate constants, and the ΔG_i represent the standard free energy gaps between the states.

from B_B to H_B compared to the $P^+B_B^-$ charge recombination rate. Given the examples cited above of electron transfer that does proceed farther along the B-side, the lack of electron transfer from B_B^- to H_B in HE(M182) is very likely due to an unfavorable free energy gap between the states $P^+B_B^-$ and $P^+H_B^-$ rather than an inherent structural constraint resulting in poor electronic coupling of the pigments. This is similar to the HL(M182) mutant, in which electron transfer does not appear to continue on from $P^+\phi_B^-$ to form $P^+H_B^-$ because of the unfavorable energetics of the charge-separated states.[17]

Relative Free Energies of B-Side Charge-Separated States. The free energy of the $P^+H_B^-$ state has not been determined experimentally. Theoretical calculations using the RC crystal structure evaluate the free energy of the $P^+H_B^-$ state 100−200 meV above the state $P^+H_A^-$.[38−40] This, in turn, would place the state $P^+H_B^-$ at most 0.1 eV below P*, as the free energy of the state $P^+H_A^-$ is estimated to be around 0.15−0.25 eV below P*.[27−30,41,42] In principle, the delayed fluorescence measurements reported in Table 1 should allow estimation of the free energy of the state $P^+B_B^-$ by comparing initial amplitudes of the fluorescence components, as has been done previously.[17,26−30] However, the situation here is more complex as the fluorescence due to recombination from the state $P^+B_B^-$ reforming P* is mixed with the faster decay components of the recombination fluorescence from the state $P^+H_A^-$, complicating this analysis somewhat.

Target Analysis of Fluorescence Kinetics. To resolve the contributions to the fluorescence from the recombination of the B- and A-side charge-separated states, fluorescence kinetics were modeled according to the kinetic scheme described in Figure 3 using target analysis.[43] As previously suggested, the multi-exponential decay of the fluorescence kinetics in WT RCs can be explained by the relaxation of the charge-separated state $P^+H_A^-$, which gives rise to a time dependent standard free energy gap between P* and $P^+H_A^-$.[27,29,44] WT RC fluorescence results have been modeled using four thermodynamically distinct states: P* and three distinct $P^+H_A^-$ states. Each of the $P^+H_A^-$ states represents a different reaction center conformation with a different free energy for the charge-separated state. In the case of the HE(M182) mutant, a fifth state, $P^+B_B^-$, was added to the model to allow for B-side electron transfer.

On the basis of the kinetic scheme shown in Figure 3, the excited and charge-separated state dynamics can be described by a system of linear differential equations. This system is fully determined if the rate constants of the different processes and the initial conditions are known. It is assumed that only P is excited and that the concentrations of all charge-separated states are initially zero. However, the rate constants for most of the reactions are not known. Thus, they were allowed to vary freely as fitting parameters to obtain the best description of the data. The actual fitting parameters employed were the forward rate constants for each reaction, the free energies between states, and the decay rate constants from the terminal charge-separated states ($P^+B_B^-$ and the lowest energy form of $P^+H_A^-$) to the ground state. A complete description of the target analysis method is presented in the Appendix A.

TABLE 2: Target Analysis Results of the Fluorescence Kinetics

sample	τ_1, ps[a]	τ_2, ps	τ_3, ns	τ_4, ns	τ_5, ps	τ_6, ps	ΔG_1, meV	ΔG_2, meV	ΔG_3, meV	ΔG_4, meV
WT	4.7	200	0.9	4	-	-	108	36	36	-
HE(M182)	3	150	1.3	6	9	65	108	35	27	70

[a] τ_1 through τ_6 are time constants that are the reciprocals of the rate constants k_1-k_6 shown in Figure 3. ΔG_1 through ΔG_4 are also defined in Figure 3. Based on the fitting accuracy, the estimated errors for the time constants are less than 10%, with the exception of τ_1 and τ_5, as their resolution is limited by the instrument response function. The ΔG_i are evaluated within ±10 meV.

The results of the target analysis are shown in Table 2. The free energy of the state $P^+B_B^-$ in the HE(M182) mutant reaction centers determined from the target analysis is about 70 ± 10 meV below P*, corresponding to an equilibrium constant between the states $P^+B_B^-$ and P* of about 15.

Target analysis is, in general, very model-dependent; thus, in evaluating the results, it is useful to look for consistency with other investigations. One would expect that the results from WT RCs would be consistent with previous analysis of the delayed fluorescence. Indeed, the 0.11 eV value of the initial free energy gap between P* and $P^+H_A^-$ and the 0.07 eV relaxation of this state on the nanosecond time scale in both WT and the HE-(M182) mutant are in good agreement with previous results.[29] Also, the agreement between the values of the A-side time constants and free energies between the HE(M182) mutant and WT RCs is consistent with the notion that the mutation primarily affects B-side parameters.

Comparison of Fluorescence Target Analysis to Transient Absorbance Data. The kinetic model used to describe the fluorescence makes an interesting prediction that can be tested by comparison to the transient absorbance data. The estimated 70 meV free energy gap between the states P* and $P^+B_B^-$ is small enough that one would expect some $P^+B_B^-$ to decay via P* forming $P^+H_A^-$ at room temperature, given the rapid rate of conversion of P* to $P^+H_A^-$ and the fact that $P^+H_A^-$ is lower in free energy than $P^+B_B^-$. This effect is indeed observed in the transient absorbance data. The decay-associated spectrum of the 45 ps component in Figure 2b shows that there is an increase in H_A bleaching. This means that, as $P^+B_B^-$ decays, some $P^+H_A^-$ is formed.

It is possible to calculate the amount of the initial $P^+B_B^-$ that should decay via each of the two paths (directly to the ground state or via P* to $P^+H_A^-$) either by considering the energetics and rate constants from the fluorescence modeling or by considering the transient absorbance data. In the fluorescence analysis (Table 2), the B-side electron-transfer rate constant was determined to be $(9\ \text{ps})^{-1}$, and the free energy gap between the states P* and $P^+B_B^-$ was 70 meV. Combining these numbers, the rate constant for the recombination reaction of $P^+B_B^-$ back to P* is calculated to be about $(140\ \text{ps})^{-1}$. The fluorescence analysis also gives a rate constant for the decay of the $P^+B_B^-$ to the ground state of $(65\ \text{ps})^{-1}$. This implies that about one-third of the initially created $P^+B_B^-$ will be converted to $P^+H_A^-$, whereas the other two-thirds will decay to the ground state.

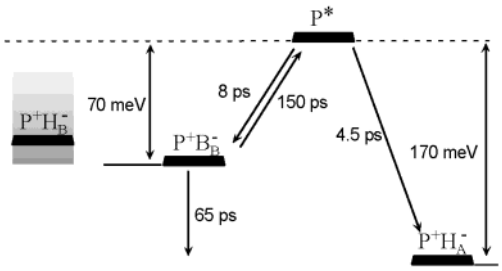

Figure 4. Schematic diagram describing the kinetic and thermodynamic parameters of the A- and B-side charge-separated states in HE(M182) mutant RCs.

A similar calculation can be done based on the transient absorbance data. In Figure 2b, the area of the H_A bleaching increase is about 15% of the total final H_A bleaching at 540 nm. Because the final yield of the state $P^+H_A^-$ is 75% of the reaction centers excited (25% decayed from $P^+B_B^-$ to the ground state), this means that $0.75 \times 0.15 = 0.11$ or about 11% of the reaction centers are involved in the conversion from $P^+B_B^-$ to $P^+H_A^-$ via P*. Comparing this to the 25% of the reaction centers that formed $P^+B_B^-$ and then decayed directly to the ground state, this again says that about two-thirds of the reaction centers that form $P^+B_B^-$ decay directly to the ground state and about one-third decay via P* to $P^+H_A^-$. This is in excellent agreement with the results of the target analysis.

From the above-mentioned values, the overall yield of $P^+B_B^-$ formation in the HE(M182) reaction centers can be estimated. As shown in Figure 2, there is about 25% of the P ground-state bleaching recovery on the 45 ps time scale. If this 25% represents two-thirds of the initial $P^+B_B^-$ formed with the other one-third (about 11−12%) being converted to $P^+H_A^-$ via P*, that means that the total yield of $P^+B_B^-$ formed on the few picosecond time scale is roughly 35% of the initial P* excited.

Knowing the yield of B-side charge separation, one can estimate the microscopic rate constants for initial electron transfer on the A- and B-sides in HE(M182) reaction centers. Combining the B-side charge separation yield with the observed 2.8 ps time constant of P* decay, the initial electron-transfer time constant on the A-side in this mutant is estimated to be about 4.5 ps and that on the B-side is about 8.0 ps, in good agreement with the 3 and 9 ps values obtained from the target analysis (see Table 2). Also, because about one-third of the $P^+B_B^-$ decays via P* to $P^+H_A^-$, the microscopic rate constants for the two $P^+B_B^-$ decay paths from the transient absorbance data can be calculated. The overall decay time of $P^+B_B^-$ is 45 ps (Figure 2), and combining these values gives a time constant of about 150 ps for $P^+B_B^-$ conversion to $P^+H_A^-$ and a time constant of about 65 ps for the direct decay of $P^+B_B^-$ to the ground state. Again, essentially the same rate constants for these decay paths were determined from the target analysis of the fluorescence kinetics (see Table 2 and above, also Figure 4). The agreement between the kinetic parameters and charge-separated state yields derived from the transient absorbance data and the target analysis of the fluorescence provides additional confidence that the value of 70 meV for the standard free energy of the B-side charge-separated state $P^+B_B^-$ in the HE(M182) mutant RCs is reliable.

Relative Standard Free Energy of $P^+H_B^-$. Given the lack of electron transfer from $P^+B_B^-$ forming $P^+H_B^-$ in the mutant, it seems likely that the standard free energy of the state $P^+H_B^-$ is as high or higher than the energy of the state $P^+B_B^-$. This is in agreement with the theoretical estimates that the $P^+H_B^-$ free energy is 100−200 meV above the $P^+H_A^-$ (i.e., at most 100 meV below P*).[38−40] Given the fact that there are mutants and other conditions in which $P^+H_B^-$ is formed from P*,[24,25,31−35] the standard free energy of $P^+H_B^-$ presumably must be lower than that of P*. This places it between 0 and 70 meV below P* (see Figure 4).

B-Side Electronic Coupling. The results from the HE(M182) mutant also provide additional evidence concerning the relative electronic coupling of the cofactors on the A- and B-sides. As discussed above, the calculated time constant for initial B-side electron transfer is about 8−9 ps. The estimated time constant is approximately two times longer than that of initial electron transfer on the A-side. If this difference were assumed to be due entirely to electronic coupling, it would correspond to a roughly 1.4-fold difference in the electronic matrix elements favoring the A-side over B-side. A very similar result was also obtained in the case of the HL(M182) mutant[17] and other mutants.[33] Apparently, the electronic coupling between electron transfer states is not very different between the A- and B-sides of the *Rb. sphaeroides* RC, in contrast to suggestions from some theoretical calculations.[45,46] The results presented here and in previous work[17,33] imply that the energies of the states $P^+B_A^-$ and $P^+B_B^-$ are the dominant factors in determining electron-transfer directionality in the bacterial reaction center.

Stabilization of B_B^- in HE(M182) Reaction Centers. An unresolved issue with regard to the HE(M182) mutation is the molecular mechanism for the apparent stabilization of B_B^- (or $P^+B_B^-$) when histidine is replaced with glutamic acid. All BChl molecules in the RCs of purple nonsulfur bacteria such as *Rb. sphaeroides*, *Rb. capsulatus*, and *Blastochloris* (*Bl.*) *viridis* are ligated by histidine residues. However, histidine is certainly not the only known ligand of BChl. In other photosynthetic pigment−protein complexes, a wide range of ligands is used for bacteriochlorophyll or chlorophyll molecules.[47−51] In bacterial reaction centers, several studies have been performed to investigate how the identity of the ligand affects the properties of the bacteriochlorophyll molecules. Most of these have been limited to the investigation of the ligands to the BChl molecules constituting the special pair P.[7−9,12−14] It was found that mutating histidine to glutamic acid at position M202 in RCs from *Rb. sphaeroides* leads to the formation of a heterodimer special pair (BPheo replaces one of the two BChl molecules constituting P). The HE(M202) mutation also shifts the P/P^+ midpoint potential by about 170 mV above the WT value.[13,14] However, the mutation HE(M182) does not result in the replacement of the BChl molecule in the B_B binding site with BPheo. This suggests that the glutamic acid side chain can be accommodated in the B_B binding pocket without creating as much steric hindrance as in the case of the HE(M202) mutation. Similarly, mutation of the histidine ligating B_A to glutamic acid in *Bl. viridis* RCs also does not cause pigment exchange.[11] This mutation causes a decrease of the P/P^+ midpoint potential by almost 50 mV, presumably because of a favorable electrostatic interaction between the glutamic acid residue and P^+. Also, the initial electron transfer reaction in this mutant was significantly altered compared to WT RC. The initial charge separation time constant increased to 12 ps and the electron-transfer yield decreased to 75%.[11] The authors argued that glutamic acid caused the energy of the state $P^+B_A^-$ to increase slightly above P*, possibly because of a negative charge on the glutamic acid interacting with B_A^-, though there was no experimental determination of the ionization state of the glutamic acid. In the case of HE(M182), there is certainly no reason to suspect that the glutamic acid at the M182 position would be negatively charged. Instead, it apparently stabilizes the $P^+B_B^-$ state, which is presumably about 0.1 eV above P* in WT RCs.[17,39] Indeed this

stabilization is quite substantial, given that, in the mutant, $P^+B_B^-$ is apparently about 70 meV below P*. The molecular interactions that allow the glutamic acid ligand to have this effect remain unknown.

Acknowledgment. This research was supported by NSF Grants MCB9817388 and MCB0131766. The transient spectrometer used was funded by the NSF Grant BIR9512970. This is publication No. 540 from the Center for the Study of Early Events in Photosynthesis.

Appendix A: Description of the Target Analysis Method

The time course of fluorescence kinetics as well as the dynamics of the electron-transfer processes in the HE(M182) mutant after excitation of the initial electron donor (see Figure 4) can be described using a system of linear equations:

$$\frac{\mathrm{d}}{\mathrm{d}t}C = AC$$

$$C = (P^* \;\; (P^+H_A^-)_1 \;\; (P^+H_A^-)_2 \;\; (P^+H_A^-)_3 \;\; P^+B_B^-)$$

$$A = \begin{bmatrix} -(k_1+k_5) & k_{1r} & 0 & 0 & k_{5r} \\ k_1 & -(k_{1r}+k_2) & k_{2r} & 0 & 0 \\ 0 & k_2 & -(k_{2r}+k_3) & k_{3r} & 0 \\ 0 & 0 & k_3 & -(k_{3r}+k_4) & 0 \\ k_5 & 0 & 0 & 0 & -(k_{5r}+k_6) \end{bmatrix}$$

where the k_i denote the forward rate constants of the electron transfer or charge-separated state ($P^+H_A^-$) relaxation processes. The rate constants with the subscript r, k_{ir}, stand for the reverse rate constants, which are related to the forward rate constants as

$$k_{ir} = k_i \exp\left(\frac{\Delta G_i}{k_B T}\right)$$

Here the ΔG_i are the free energy gaps between the states, k_B is Boltzmann's constant, and T is temperature.

The general solution of this system of equations can be written as

$$C_i(t) = \sum_j a_{ij} \exp(-\lambda_j t)$$

where λ_j are the eigenvalues of the rate constant matrix **A** and the matrix of the amplitudes a_{ij} is explicitly determined by the initial conditions:

$$a = J^{-1} \cdot D \cdot J$$

Here, J is the matrix made up of the columns of matrix **A** eigenvectors and D is the vector describing initial conditions. In the present case, only P* is initially excited and concentrations of other states are equal to 0 (i.e., $D = [1, 0, 0, 0, 0]$). Thus, the only parameters determining the dynamics of the system are the rate constants k_i and the free energy gaps ΔG_i.

The parameters that best describe the system can be found by fitting them using nonlinear least-squares methods employing theoretical fluorescence decay curves

$$F(t) = C(t) \otimes \mathrm{IRF}(t)$$

Here, IRF(t) stands for the measured instrument response function, which is convoluted with the pure exponential decay $C(t)$. In the case of the investigated system (see Figure 3), the only fluorescent state is P* which tremendously simplifies the fitting procedure.

References and Notes

(1) Woodbury, N. W.; Allen, J. P. The pathway, kinetics and thermodynamics of electron transfer in wild type and mutant reaction centers of purple nonsulfur bacteria. In *Anoxygenic Photosynthetic Bacteria*; Blankenship, R. E., Madigan, M. T., Bauer, C. E., Eds.; Kluwer Academic Publishers: Dordrecht, 1995; Vol. 2, pp 527−557.

(2) Parson, W. W. Photosynthetic bacterial reaction centres. In *Protein Electron Transfer*; Bendall, S. D., Ed.; BIOS scientific publishers: Oxford, 1996; pp 125−160.

(3) Hoff, A. J.; Deisenhofer, J. *Phys. Rep.* **1997**, *287*, 1−247.

(4) Wraight, C. A.; Clayton, R. K. *Biochim. Biophys. Acta* **1973**, *333*, 246−260.

(5) Kirmaier, C.; Holten, D.; Parson, W. W. *Biochim. Biophys. Acta* **1985**, *810*, 49−61.

(6) Kirmaier, C.; Holten, D.; Parson, W. W. *Biochim. Biophys. Acta* **1985**, *810*, 33−48.

(7) Bylina, E. J.; Youvan, D. C. *Proc. Natl. Acad. Sci. U.S.A.* **1988**, *85*, 7226−7230.

(8) Breton, J.; Bylina, E. J.; Youvan, D. C. *Biochemistry* **1989**, *28*, 6423−6430.

(9) Bylina, E. J.; Kolaczkowski, S. V.; Norris, J. R.; Youvan, D. C. *Biochemistry* **1990**, *29*, 6203−6210.

(10) Gallo, D. M., Jr.; Taguchi, A. K. W.; Woodbury, N. W. *Biophys. J.* **1994**, *66*, A126.

(11) Arlt, T.; Dohse, B.; Schmidt, S.; Wachtveitl, J.; Laussermair, E.; Zinth, W.; Oesterhelt, D. *Biochemistry* **1996**, *35*, 9235−9244.

(12) Goldsmith, J. O.; King, B.; Boxer, S. G. *Biochemistry* **1996**, *35*, 2421−2428.

(13) Schulz, C.; Muh, F.; Beyer, A.; Jordan, R.; Schlodder, E.; Lubitz, W. Investigation of *Rhodobacter sphaeroides* reaction center mutants with changed ligands to the primary donor. In *Photosynthesis*: *Mechanisms and Effects*; Garab, G., Ed.; Kluwer Academic Publishers: The Netherlands, 1998; Vol. 2, pp 767−770.

(14) Nabedryk, E.; Schulz, C.; Muh, F.; Lubitz, W.; Breton, J. *Photochem. Photobiol.* **2000**, *71*, 582−588.

(15) Gallo, D. M., Jr. Chimeric mutagenesis of the *Rb. capsulatus* reaction center: An exploration of the structure/function relationship. Ph.D. Thesis, Arizona State University, Tempe, AZ, 1994.

(16) Katilius, E.; Turanchik, T.; Lin, S.; Taguchi, A. K. W.; Woodbury, N. W. *J. Phys. Chem. B* **1999**, *103*, 7386-7389.

(17) Katilius, E.; Katiliene, Z.; Lin, S.; Taguchi, A. K. W.; Woodbury, N. W. *J. Phys. Chem. B* **2002**, *106*, 1471−1475.

(18) Williams, J. C.; Taguchi, A. K. W. Genetic manipulation of purple photosynthetic bacteria. In *Anoxygenic Photosynthetic Bacteria*; Blankenship, R. E., Madigan, M. T., Bauer, C. E., Eds.; Kluwer Academic Publishers: Dordrecht, 1995; Vol. 2, pp 1029−1065.

(19) Lin, X.; Williams, J. C.; Allen, J. P.; Mathis, P. *Biochemistry* **1994**, *33*, 13517−13523.

(20) Kirmaier, C.; Holten, D. *Photosynth. Res.* **1987**, *13*, 225−260.

(21) Kennis, J. T. M.; Shkuropatov, A. Y.; van Stokkum, I. H. M.; Gast, P.; Hoff, A. J.; Shuvalov, V. A.; Aartsma, T. J. *Biochemistry* **1997**, *36*, 16231−16238.

(22) Kirmaier, C.; Gaul, D.; DeBey, R.; Holten, D.; Schenck, C. C. *Science* **1991**, *251*, 922−927.

(23) Robert, B.; Lutz, M.; Tiede, D. M. *FEBS Lett.* **1985**, *183*, 326−330.

(24) Heller, B. A.; Holten, D.; Kirmaier, C. *Science* **1995**, *269*, 940−945.

(25) Kirmaier, C.; Cua, A.; He, C.; Holten, D.; Bocian, D. F. *J. Phys. Chem. B* **2002**, *106*, 495−503.

(26) Arata, H.; Parson, W. W. *Biochim. Biophys. Acta* **1981**, *638*, 201−209.

(27) Schenck, C. C.; Blankenship, R. E.; Parson, W. W. *Biochim. Biophys. Acta* **1982**, *680*, 44−59.

(28) Woodbury, N. W. T.; Parson, W. W. *Biochim. Biophys. Acta* **1984**, *767*, 345−361.

(29) Peloquin, J. M.; Williams, J. C.; Lin, X.; Alden, R. G.; Murchison, H. A.; Taguchi, A. K. W.; Allen, J. P.; Woodbury, N. W. *Biochemistry* **1994**, *33*, 8089−8100.

(30) Ogrodnik, A.; Hartwich, G.; Lossau, H.; Michel-Beyerle, M. E. *Chem. Phys.* **1999**, *244*, 461−478.

(31) Laible, P. D.; Kirmaier, C.; Holten, D.; Tiede, D. M.; Schiffer, M.; Hanson, D. K. Formation of $P^+Q_B^-$ via B-branch electron transfer in mutant reaction centers. In *Photosynthesis*: *Mechanisms and Effects*; Garab, G., Ed.; Kluwer Academic Publishers: The Netherlands, 1998; Vol. 2, pp 849−852.

(32) Kirmaier, C.; Weems, D.; Holten, D. *Biochemistry* **1999**, *38*, 11516−11530.

(33) Kirmaier, C.; He, C.; Holten, D. *Biochemistry* **2001**, *40*, 12132−12139.

(34) Roberts, J. A.; Holten, D.; Kirmaier, C. *J. Phys. Chem. B* **2001**, *105*, 5575−5584.

(35) Kirmaier, C.; Laible, P. D.; Czarnecki, K.; Hata, A. N.; Hanson, D. K.; Bocian, D. F.; Holten, D. *J. Phys. Chem. B* **2002**, *106*, 1799−1808.

(36) Lin, S.; Jackson, J. A.; Taguchi, A. K. W.; Woodbury, N. W. *J. Phys. Chem. B* **1999**, *103*, 4757−4763.

(37) Lin, S.; Katilius, E.; Haffa, A. L. M.; Taguchi, A. K. W.; Woodbury, N. W. *Biochemistry* **2001**, *40*, 13767−13773.

(38) Michel-Beyerle, M. E.; Plato, M.; Deisenhofer, J.; Michel, H.; Bixon, M.; Jortner, J. *Biochim. Biophys. Acta* **1988**, *932*, 52−70.

(39) Parson, W. W.; Chu, Z.-T.; Warshel, A. *Biochim. Biophys. Acta* **1990**, *1017*, 251−272.

(40) Gunner, M. R.; Nicholls, A.; Honig, B. *J. Phys. Chem.* **1996**, *100*, 4277−4291.

(41) Ogrodnik, A.; Volk, M.; Letterer, R.; Feick, R.; Michel-Beyerle, M. E. *Biochim. Biophys. Acta* **1988**, *936*, 361−371.

(42) Ogrodnik, A.; Keupp, W.; Volk, M.; Aumeier, G.; Michel-Beyerle, M. E. *J. Phys. Chem.* **1994**, *98*, 3432−3439.

(43) Holzwarth, A. R. Data Analysis of Time − Resolved Measurements. In *Biophysical Techniques in Photosynthesis*; Amesz, J., Hoff, A. J., Eds.; Kluwer Academic Publisher: Netherlands, 1996; pp 75−92.

(44) Trissl, H. W.; Bernhardt, K.; Lapin, M. *Biochemistry* **2001**, *40*, 5290−5298.

(45) Kolbasov, D.; Scherz, A. Matrix elements play a significant role in asymmetric electron transfer in bacterial reaction centers. In *Photosynthesis*: *Mechanisms and Effects*; Garab, G., Ed.; Kluwer Academic Publishers: The Netherlands, 1998; Vol. 2, pp 719−722.

(46) Kolbasov, D.; Scherz, A. *J. Phys. Chem. B* **2000**, *104*, 1802−1809.

(47) Tronrud, D. E.; Schmid, M. F.; Matthews, B. W. *J. Mol. Biol.* **1986**, *188*, 443−454.

(48) Kuhlbrandt, W.; Wang, D. N.; Fujiyoshi, Y. *Nature* **1994**, *367*, 614−621.

(49) McDermott, G.; Prince, S. M.; Freer, A. A.; Hawthornthwaite-Lawless, A. M.; Papiz, M. Z.; Cogdell, R. J.; Isaacs, N. W. *Nature* **1995**, *374*, 517−521.

(50) Li, Y. F.; Zhou, W. L.; Blankenship, R. E.; Allen, J. P. *J. Mol. Biol.* **1997**, *271*, 456−471.

(51) Jordan, P.; Fromme, P.; Witt, H. T.; Klukas, O.; Saenger, W.; Kraus, N. *Nature* **2001**, *411*, 909−917.